Trajectory tracking for aerobatics maneuvers in quadrotors vehicle

E. Ibarra, Pedro Castillo Garcia

Trajectory tracking for aerobatics maneuvers in quadrotors vehicle

E. Ibarra[2] and Pedro Castillo[1,2]

***Abstract*— Some inspection missions for quadrotors require a previous definition of the trajectories before being tracked. The well design of the trajectory can contribute for the success of the mission when aggressive maneuvers are demanded. In this paper, we propose a solution for designing and tracking unconventional trajectories requiring aerobatics maneuvers in quadrotors. The trajectory is based on the Hopf bifurcations and the sliding mode approach to form spiral loops in 3D around a pillar that need to be inspected by a quadrotor. The control architecture is based on the sliding mode methodology adding new parameters for achieving a desired angular velocity around the stable limit cycle solution. The proposed solution is validated in simulations and numerical results illustrate the good performance of the proposed trajectory-tracking control scheme.**

I. INTRODUCTION

Surveillance and inspection tasks become popular for aerial vehicles, specially for quadrotors. Such missions are defined in a classical way (waypoints, etc.) and the challenge here is to keep the aerial vehicle at hover in presence of external perturbations. Avances in technology give us the opportunity to develop more complex missions for the UAVs (Unmanned Aerial Vehicles), improving significantly their maneuvers.

Aerial path following is not a new challenge and it has been studied since several years. Nevertheless the trajectories are classical or in most cases they are defined in the horizontal plane, see [1]. For example, in [2] a controller is proposed for path-following under different parameter settings and wind disturbances. The obtained results are interesting nevertheless the proposed trajectory is developed in the horizontal plane. In [3], the author proposes a flight control system capable to stabilize attitude and tracking a trajectory accurately using a quadrotor vehicle. Simulation results validate the proposed controller, nevertheless, from figures it can observed that the trajectory is a square in 3D and the vehicle performs only vertical and lateral displacement keeping the orientation to zero. [4] have developed a nonlinear control based on H_∞ to solve the path tracking problem for a quadrotor. The algorithm was validated in simulation when the quadrotor follows a spiral trajectory. This trajectory does not requires bigger changes in the orientation, reducing the problem to making circles in a plane and moving in the z axis. In [5], authors solve the problem of position trajectory-tracking and path-following control design for underactuated autonomous vehicles in the presence of possibly large modeling parametric uncertainties. The algorithm was validated in simulations when the vehicle is moving in 2D or 3D space. The trajectory used is a smooth bounded curve parameterized by time. Similarly, [6] have developed a method for accurate path following for miniature air vehicles. The method is based on the notion of vector fields, which are used to generate desired course inputs to inner-loop attitude control laws. Experimental results have demonstrated the good performance of the controller, nevertheless the trajectory is defined only in the horizontal plane.

In [9] the problem of constrained nonlinear trajectory tracking control for UAVs is studied. Nevertheless, the approach is validated in simulation with conservative trajectories. In [8] the authors have investigated the feasibility of a nonlinear model predictive tracking control (NMPTC) for autonomous helicopters. The controller was implemented an on-line optimization controller using gradient-descent method. A circular trajectory is used in [7] for validating a nonlinear control algorithm based on vision measurements. The control performs well in simulation holding the quadrotor orientation stable.

New complex trajectories are now being designed for other kind of aerial missions, see [10], [11], [12], [15], [13], [14]. In [12] a detailed comparison between two state-of-the-art model-based control techniques (Linear Model Predictive Controller (LMPC) vs Nonlinear Model Predictive Controller (NMPC) for MAV trajectory tracking is presented. The authors validated their results in real-time nevertheless, they assume that the vehicle attitude is controlled by an attitude controller which simplify the control problem. In [15] the authors addressed a practical approach for optimal trajectory tracking allowing distributed collision avoidance for multiple unmanned aerial vehicles sharing the same workspace. The solution is interesting nevertheless, authors focalized again only in translation mouvements. In [13], an improved adaptive sliding mode (IASMC) control strategy was developed to control the quadcopter's attitude, while an interval type-2 fuzzy PID (IT2-FPID) controller was adopted to control the quadcopter's position for trajectory tracking. The controllers were validated in simulations without important changes in the attitude system. Finally in [14] authors pursued a model-independent solution to the coordinated trajectory-tracking control (CTTC) problem, whereby the USV unmanned surface vehicle) is noncooperative with a quadrotor. Even if in this work, authors proposed trajectory tracking they focus in solutions for uncertainties, complex unknowns, nonlinear dynamics, disturbances, and intermediate signals.

[1]Corresponding author

[2]E. Ibarras is at Instituto tecnologico de Durango, México and P. Castillo is with the Université de technologie de Compiègne, CNRS, Heudiasyc (Heuristics and Diagnosis of Complex Systems), CS 60 319 - 60 203 Compiègne Cedex, France efraibarrajimenez@gmail.com, castillo@hds.utc.fr

In this work, a non-conventional trajectory for aerial inspection missions in 3D is conceived. The trajectory has some properties that increases the maneuverability of the aerial vehicle to perform acrobatic maneuvers. For designing the trajectory ideas from the bifurcation theory ([17], [18], [16]) and the concept of the sliding surfaces ([19], [20], [21]) are considered. In addition, flight properties (nonlinear dynamics) and constraints (initial conditions, etc) of the aerial vehicle are taken into account when the trajectory is conceived for 3D movements. A nonlinear controller based on the integral sliding mode technique is developed to assure the trajectory tracking and to achieve robustness since the beginning.

This solution can be used for different applications where aerial agressive acrobatic maneuvers are needed. For example, for inspecting a pillar, see Figure 1, some constraints are imposed (the quadrotor needs to point its frontal camera all time to the pillar for inspect it) and need to be abided by the controller.

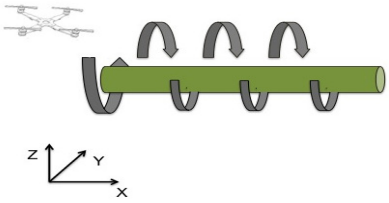

Fig. 1. Inspection mission with acrobatic maneuvers.

This paper is organized as follows; some preliminaries notions for designing the trajectory are given in section II. The trajectory is conceived and explained with details in section III. The nonlinear controller is developed in section IV. Simulation results showing the good performance of the controller when tracking the trajectory are also depicted in this section. Finally, conclusions about this work are discussed in section V.

II. Preliminaries

In books of nonlinear ordinary differential equations as for example [17], [18], [16], when the term bifurcation parameter μ is mentioned, it is referred to describe the type of stable or unstable solutions around equilibrium points or also stable or unstable solutions around isolated closed paths, commonly named limit cycles. As a consequence, the type of stability is determinated by considering the parameter $\mu < 0$, $\mu = 0$ & $\mu > 0$. For example; consider the system given by $\dot{x} = y, \quad \dot{y} = \mu x$ with $\mu \in (-\infty, \infty)$. The phase diagram contains a center for $\mu < 0$ and a saddle for $\mu > 0$, these classifications representing radically different types of stable and unstable system behaviors. The change in stability occurs when $\mu = 0$ meaning that a bifurcation occurs.

Note that the limit cycles can only occur in nonlinear differential equation as for example

$$\begin{aligned} \dot{x} &= \mu x + \gamma y - x(x^2 + y^2) \\ \dot{y} &= -\gamma x + \mu y - y(x^2 + y^2) \end{aligned} \tag{1}$$

where μ and γ are constant parameters and x, y are states of the system. The previous system has a single equilibrium point at the origin. This system can be represented in polar coordinates defining $r^2 = x^2 + y^2$ and $\tan(\chi) = \dfrac{y}{x}$, implying that $x = r\cos(\chi)$ and $y = r\sin(\chi)$. And then

$$\dot{r} = r\left(\mu - r^2\right), \quad \dot{\chi} = -\gamma. \tag{2}$$

One particular solution is $r = \sqrt{\mu}$ and $\chi = -\gamma t$, that corresponds to the limit cycle, $x = \sqrt{\mu}\cos(\gamma t)$ and $y = -\sqrt{\mu}\sin(\gamma t)$ with t is the time. Also $\dot{r} > 0$ when $0 < r < \sqrt{\mu}$ and $\dot{r} < 0$ when $r > \sqrt{\mu}$. Observe that if $\mu \leq 0$, then the entire diagram consists of a stable spiral at the origin. If $\mu > 0$ then there is a unstable spiral at the origin surrounded by a stable limit cycle which grows out of the origin. Notice that when the parameter μ generates a limit cycle, the Hopf bifurcation appears. The stability cases with parameters $\mu < 0$, $\mu = 0$ & $\mu > 0$, with $\gamma > 0$ & $\gamma < 0$ respectively are shown in Figure 2. Notice from this figure that the parameter γ is not a bifurcation parameter cause it only produces a steady clockwise spiral motion if $\gamma > 0$, and a steady counterclockwise spiral motion if $\gamma < 0$.

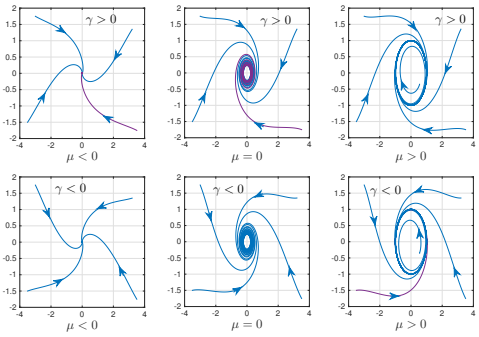

Fig. 2. Development of a limit cycle in a Hopf bifurcation.

III. Trajectory design for acrobatic maneuvers

Consider that the X axis of the inertial frame is placed on the longitudinal part of the pillar as can be appreciated in Figure 1. Therefore, analyzing the plane (Y, Z) the challenge will be to obtain a nonlinear system based on (1) that can guarantee to establish a desired radius r as well as an angular velocity around an equilibrium point (h, k). This radius will define the desired position for the aerial vehicle in the coordinates Y, Z.

Hence, defining y_{1_r} and z_{1_r} as the desired position of the vehicle, then

$$\begin{aligned} \dot{y}_{1_r} &= \mu y_{1_r} + \gamma\, z_{1_r} - y_{1_r}\left(y_{1_r}^2 + z_{1_r}^2\right) \\ \dot{z}_{1_r} &= -\gamma\, y_{1_r} + \mu z_{1_r} - z_{1_r}\left(y_{1_r}^2 + z_{1_r}^2\right). \end{aligned} \tag{3}$$

Notice that the mission requires agressive maneuvers around the pillar, for this, we will focus in the bifurcation parameter $\mu > 0$ to generate a limit cycle around the origin. However the goal will be to have it around any point (h, k)

thus define $e_{y_{1_r}} = y_{1_r} - h$ and $e_{z_{1_r}} = z_{1_r} - k$ and it follows that

$$\begin{aligned} \dot{e}_{y_{1_r}} &= \mu e_{y_{1_r}} + \gamma e_{z_{1_r}} - e_{y_{1_r}} \left(e_{y_{1_r}}^2 + e_{z_{1_r}}^2 \right) \\ \dot{e}_{z_{1_r}} &= -\gamma e_{y_{1_r}} + \mu e_{z_{1_r}} - e_{z_{1_r}} \left(e_{y_{1_r}}^2 + e_{z_{1_r}}^2 \right) \end{aligned} \tag{4}$$

with the limit cycle defined as (see Figure 3)

$$\begin{aligned} y_{1_r} &= h + \sqrt{\mu} \cos(\gamma t) \\ z_{1_r} &= k - \sqrt{\mu} \sin(\gamma t) . \end{aligned}$$

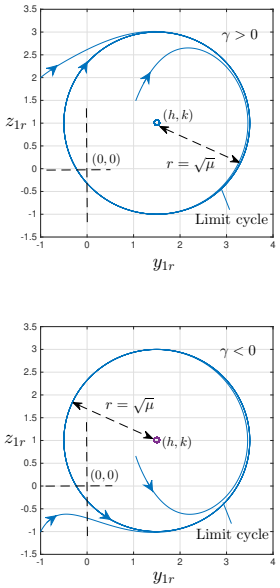

Fig. 3. Approach of two phase paths to the stable limit cycle $(y_{1_r} - h)^2 + (z_{1_r} - k)^2 = \mu$, with $\dot{\chi} = -\gamma$

Observe from Figure 3 that the paths approach the limit cycle from both sides, if $\gamma > 0$ a steady clockwise spiral motion is presented. Similarly, if $\gamma < 0$ a steady counter-clockwise spiral motion appears around the limit cycle.

Assuming that (h, k) are constant thus, system (4) can also be written as

$$\begin{aligned} \dot{y}_{1_r} &= \mu e_{y_{1_r}} + \gamma e_{z_{1_r}} - e_{y_{1_r}} \left(e_{y_{1_r}}^2 + e_{z_{1_r}}^2 \right) \\ \dot{z}_{1_r} &= -\gamma e_{y_{1_r}} + \mu e_{z_{1_r}} - e_{z_{1_r}} \left(e_{y_{1_r}}^2 + e_{z_{1_r}}^2 \right) \end{aligned} \tag{5}$$

The initial conditions for position are given by $(y_{1_{r_0}}, z_{1_{r_0}})$, then $e_{y_{1_{r_0}}} = y_{1_{r_0}} - h$ and $e_{z1r0} = z_{1_{r_0}} - k$. Nevertheless from (5) the initial conditions for the velocity $(y_{2_{r_0}}, z_{2_{r_0}})$ are

$$\begin{aligned} y_{2_{r_0}} &= \mu e_{y_{1_{r_0}}} + \gamma e_{z_{1_{r_0}}} - e_{y_{1_{r_0}}} \left(e_{y_{1_{r_0}}}^2 + e_{z_{1_{r_0}}}^2 \right) \\ z_{2_{r_0}} &= -\gamma e_{y_{1_{r_0}}} + \mu e_{z_{1_{r_0}}} - e_{z_{1_{r_0}}} \left(e_{y_{1_{r_0}}}^2 + e_{z_{1_{r_0}}}^2 \right) \end{aligned} \tag{6}$$

with $\mu, \gamma, y_{1_{r_0}}, z_{1_{r_0}}$ dependency, that could produce high initial values for the velocity.

Initial independent conditions

The concept of sliding surface is used for rewriting equations in (5) and allowing the aerial vehicle to have initial independent conditions in its velocity. Consider the following system

$$\begin{aligned} \dot{y}_{1_r} &= y_{2_r} \qquad \dot{z}_{1_r} = z_{2_r} \\ \dot{y}_{2_r} &= u_y \qquad \dot{z}_{2_r} = u_z \end{aligned} \tag{7}$$

and define the sliding surfaces, S_y, S_z as

$$\begin{aligned} S_y &= y_{2_r} - \mu e_{y_{1_r}} - \gamma e_{z_{1_r}} + e_{y_{1_r}} \left(e_{y_{1_r}}^2 + e_{z_{1_r}}^2 \right) \\ S_z &= z_{2_r} + \gamma e_{y_{1_r}} - \mu e_{z_{1_r}} + e_{z_{1_r}} \left(e_{y_{1_r}}^2 + e_{z_{1_r}}^2 \right) \end{aligned} \tag{8}$$

where u_y and u_z will be defined later to assure $S_i \to 0$ asymptotically and choose freely $(y_{2_{r_0}}, z_{2_{r_0}})$. Derivating (8) with respect to time, it results

$$\begin{aligned} \dot{S}_y &= u_y + \left(3e_{y_{1_r}}^2 + e_{z_{1_r}}^2 - \mu \right) y_{2_r} + \left(2e_{y_{1_r}} e_{z_{1_r}} - \gamma \right) z_{2_r} \\ \dot{S}_z &= u_z + \left(\gamma + 2e_{y_{1_r}} e_{z_{1_r}} \right) y_{2_r} + \left(3e_{z_{1_r}}^2 + e_{y_{1_r}}^2 - \mu \right) z_{2_r} \end{aligned}$$

Thus, propose

$$\begin{aligned} u_y &= -\left(3e_{y_{1_r}}^2 + e_{z_{1_r}}^2 - \mu \right) y_{2_r} - \left(2e_{y_{1_r}} e_{z_{1_r}} - \gamma \right) z_{2_r} - k_y S_y \\ u_z &= -\left(\gamma + 2e_{y_{1_r}} e_{z_{1_r}} \right) y_{2_r} - \left(3e_{z_{1_r}}^2 + e_{y_{1_r}}^2 - \mu \right) z_{2_r} - k_z S_z . \end{aligned}$$

then it yields,

$$\dot{S}_y = -k_y S_y; \qquad \dot{S}_z = -k_z S_z \tag{9}$$

with $k_y, k_z > 0$. Solving the previous equations, the solutions are

$$S_y(t) = e^{-k_y t} S_y(0); \qquad S_z(t) = e^{-k_z t} S_z(0) \tag{10}$$

where $S_y(t)$, $S_z(t) \to 0$ when $t \to \infty$. Notice that (8) is equivalent to

$$\begin{aligned} \dot{y}_{1_r} &= S_y + \mu e_{y_{1_r}} + \gamma e_{z_{1_r}} - e_{y_{1_r}} \left(e_{y_{1_r}}^2 + e_{z_{1_r}}^2 \right) \\ \dot{z}_{1_r} &= S_z - \gamma e_{y_{1_r}} + \mu e_{z_{1_r}} - e_{z_{1_r}} \left(e_{y_{1_r}}^2 + e_{z_{1_r}}^2 \right) \end{aligned} \tag{11}$$

and rewriting in polar coordinates, it follows that

$$\begin{aligned} \dot{r} &= S_y \cos(\chi) + S_z \sin(\chi) + r \left(\mu - r^2 \right) \\ \dot{\chi} &= \frac{1}{r} S_z \cos(\chi) - \frac{1}{r} S_y \sin(\chi) - \gamma . \end{aligned} \tag{12}$$

A particular solution is $r = \sqrt{\mu}$ and $\chi = -\gamma\, t$ as in (2).

3D trajectory

For the inspection task, the aerial vehicle must move from an initial position $x_{1_r}(0) = x_{1_{r_0}}$ to a constant desired position x_{eq}, i.e., $e_{x_{1_r}} = x_{1_r} - x_{eq} \to 0$ when $t \to \infty$. Then, define

$$\begin{aligned} \dot{e}_{x_{1_r}} &= e_{x_{2_r}} \\ \dot{e}_{x_{2_r}} &= u_x \end{aligned} \tag{13}$$

Propose $S_x = \dot{e}_{x_{1_r}} + c e_{x_{1_r}}$ with $c > 0$, thus $\dot{S}_x = u_x + c\, e_{x_{2_r}}$ and designing $u_x = -c\, e_{x_{2_r}} - k_x S_x$, with $K_x > 0$, it follows that $\dot{S}_x = -K_x S_x$, where the solution is given by $S_x(t) = \exp(-K_x\, t)\, S_x(0)$ that it is an asymptotic stable

solution. And this implies that $e_{x_{1r}} \to 0$ and $e_{x_{2r}} \to 0$ when $t \to \infty$. Also observe that (13) is equivalent to

$$\begin{aligned} \dot{x}_{1r} &= x_{2r} \\ \dot{x}_{2r} &= u_x \end{aligned} \tag{14}$$

where $u_x = -c\, e_{x_{2r}} - k_x S_x$, with $k_x > 0$, achieves to do $x_{1r} \to x_{eq}$ and $x_{2r} \to 0$ when $t \to \infty$. Notice that u_x can be expressed as

$$u_x = -\underbrace{k_x\, c}_{k_{p_x}} e_{x_{1r}} - \underbrace{(c + k_x)}_{k_{d_x}} e_{x_{2r}} \tag{15}$$

where k_{p_x} and k_{d_x} are positive constants.

Therefore, the trajectory for acrobatic mission inspection in 3D is given by

$$\begin{aligned} \dot{x}_{1r} &= x_{2r} & \dot{x}_{2r} &= u_x \\ \dot{y}_{1r} &= y_{2r} & \dot{y}_{2r} &= u_y \\ \dot{z}_{1r} &= z_{2r} & \dot{z}_{2r} &= u_z \end{aligned} \tag{16}$$

where u_x, u_y, u_z are defined as

$$\begin{aligned} u_x &= -c\, x_{2_r} - k_x S_x \\ u_y &= -\left(3e_{y_{1_r}}^2 + e_{z_{1_r}}^2 - \mu\right) y_{2_r} - \left(2e_{y_{1_r}} e_{z_{1_r}} - \gamma\right) z_{2_r} - k_y \\ u_z &= -\left(\gamma + 2e_{y_{1_r}} e_{z_{1_r}}\right) y_{2_r} - \left(3e_{z_{1_r}}^2 + e_{y_{1_r}}^2 - \mu\right) z_{2_r} - k_z \end{aligned}$$

with S_i, $i : x, y, z$, proposed as

$$\begin{aligned} S_x &= x_{2_r} + c e_{x_{1_r}} \\ S_y &= y_{2_r} - \mu e_{y_{1_r}} - \gamma e_{z_{1_r}} + e_{y_{1_r}} \left(e_{y_{1_r}}^2 + e_{z_{1_r}}^2\right) \\ S_z &= z_{2_r} + \gamma e_{y_{1_r}} - \mu e_{z_{1_r}} + e_{z_{1_r}} \left(e_{y_{1_r}}^2 + e_{z_{1_r}}^2\right) \end{aligned}$$

with positive coefficients c, k_x, k_y, k_z and $\gamma > 0$ or $\gamma < 0$ depending of the sense of turning around the limt cycle $(y_{1r} - y_{eq})^2 + (z_{1r} - z_{eq})^2 = \mu$.

Numerical validation

Suppose that the aerial vehicle needs to inspect a tube with coordinates $(-9, 10, 3.5)$ m in its center and with $r = 1$m. Thus, the trajectory conditions are: equilibrium reference at $(x_{eq}, y_{eq}, z_{eq}) = (-9, 10, 3.5)$ m, initial position $(x_{1r}(0), y_{1r}(0), z_{1r}(0)) = (-3, 5, 0)$ m and initial velocity $(x_{2r}(0), y_{2r}(0), z_{2r}(0)) = (0, 0, 0)$ m/s with $\gamma = -4$ and $\mu = 4$, and coefficients $c = 0.75$, $k_x = 0.4$, $k_y = 2$, $k_z = 2$. The initial position could change as desired by the user, μ is chosen to be $r = 2$m that it is bigger than radios tube. Observe from Figure 4, that using (16) the trajectory is designed pretty well.

Notice from Figure 5 the asymptotic convergence of S_x, S_y, S_z to zero, which this means that $x_{1r} \to x_{eq} = -9$ when $S_x \to 0$ asymptotically, and the dynamics (y_{1r}, z_{1r}) will approach to the stable limit cycle $(y_{1r} - 10)^2 + (z_{1r} - 3.5)^2 = 4$ when simultaneously S_y, $S_z \to 0$ asymptotically.

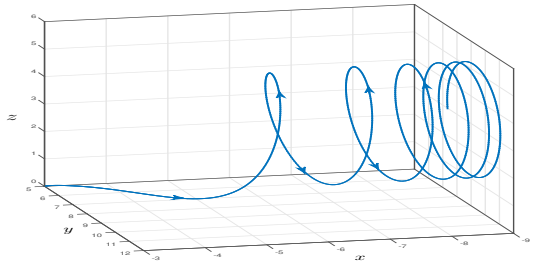

Fig. 4. Desired trajectory $(x_{1_r}, y_{1_r}, z_{1_r})$ in looping spiral.

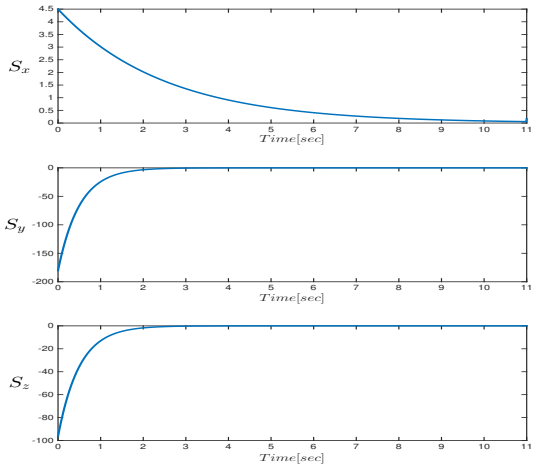

Fig. 5. Asymptotic convergence of S_x, S_y and S_z

Return to the base station

In the aerial mission, once the inspection task is done in some time T_{F_1}, the aerial vehicle needs to return to the base station, for our study it is considered to be at the initial position. Observe that at time T_{F_1} the initial conditions are given by $(x_{1r}(T_{F_1}), y_{1r}(T_{F_1}), z_{1r}(T_{F_1}))$ and $(x_{2r}(T_{F_1}), y_{2r}(T_{F_1}), z_{2r}(T_{F_1}))$ respectively. Thus, define the next errors

$$\begin{aligned} \tilde{e}_{x_{1r}} &= x_{1r} - x_{1r}(0); & \dot{\tilde{e}}_{x_{1r}} &= \tilde{e}_{x_{2r}} = x_{2r} \\ \tilde{e}_{y_{1r}} &= y_{1r} - y_{1r}(0); & \dot{\tilde{e}}_{y_{1r}} &= \tilde{e}_{y_{2r}} = y_{2r} \\ \tilde{e}_{z_{1r}} &= z_{1r} - z_{1r}(0); & \dot{\tilde{e}}_{z_{1r}} &= \tilde{e}_{z_{2r}} = z_{2r} \end{aligned}$$

Therefore the goal will be that at interval time $T_{F_1} \leq t \leq T_F$, $\tilde{e}_{x_{1r}}$, $\tilde{e}_{y_{1r}}$, $\tilde{e}_{z_{1r}}$ and $\tilde{e}_{x_{2r}}$, $\tilde{e}_{y_{2r}}$, $\tilde{e}_{z_{2r}}$ approach to zero asymptotically. Propose the following differential equations

$$\begin{aligned} \dot{\tilde{e}}_{x_{1r}} &= \tilde{e}_{x_{2r}} & \dot{\tilde{e}}_{y_{1r}} &= \tilde{e}_{y_{2r}} & \dot{\tilde{e}}_{z_{1r}} &= \tilde{e}_{z_{2r}} \\ \dot{\tilde{e}}_{x_{2r}} &= \tilde{u}_x & \dot{\tilde{e}}_{y_{2r}} &= \tilde{u}_y & \dot{\tilde{e}}_{z_{2r}} &= \tilde{u}_z \end{aligned} \tag{17}$$

where $\tilde{u}_x$, $\tilde{u}_y$, $\tilde{u}_z$ are the control inputs to achieve asymptotic convergence of the errors.

Now define the following variables σ_x, σ_y, σ_z and their derivatives $\dot{\sigma}_x$, $\dot{\sigma}_y$, $\dot{\sigma}_z$ as

$$\begin{aligned} \sigma_x &= \tilde{e}_{x_{2r}} + \tilde{c}\, \tilde{e}_{x_{1r}} & \sigma_y &= \tilde{e}_{y_{2r}} + \tilde{b}\, \tilde{e}_{y_{1r}} & \sigma_z &= \tilde{e}_{z_{2r}} + \tilde{d}\, \tilde{e}_{z_{1r}} \\ \dot{\sigma}_x &= \tilde{u}_x + \tilde{c}\, \tilde{e}_{x_{2r}} & \dot{\sigma}_y &= \tilde{u}_y + \tilde{b}\, \tilde{e}_{y_{2r}} & \dot{\sigma}_z &= \tilde{u}_z + \tilde{d}\, \tilde{e}_{z_{2r}} \end{aligned}$$

with positive gains $\tilde{c}$, $\tilde{b}$, $\tilde{d}$. Proposing the control inputs $\tilde{u}_x$, $\tilde{u}_y$, $\tilde{u}_z$ as

$$\begin{aligned}\tilde{u}_x &= -\tilde{c}\,\tilde{e}_{x_{2r}} - \tilde{k}_x\sigma_x \\ \tilde{u}_y &= -\tilde{b}\,\tilde{e}_{y_{2r}} - \tilde{k}_y\sigma_y \\ \tilde{u}_z &= -\tilde{d}\,\tilde{e}_{z_{2r}} - \tilde{k}_z\sigma_z\end{aligned} \tag{18}$$

with $\tilde{k}_i > 0$, it follows that

$$\dot{\sigma}_x = -\tilde{k}_x\sigma_x, \quad \dot{\sigma}_y = -\tilde{k}_y\sigma_y, \quad \dot{\sigma}_z = -\tilde{k}_z\sigma_z \tag{19}$$

where the solutions at the interval time $T_{F_1} \leq t \leq T_F$ will be given as $\sigma_i(t) = \exp\left(-\tilde{k}_i\,(t - T_{F_1})\right)\sigma_i(T_{F_1})$, $i : x, y, z$, implying that σ_i is an asymptotically stable solution. Notice that if $t \to T_F$, with $T_F = \infty$, then this means that $\sigma_x \to 0, \sigma_y \to 0$, $\sigma_z \to 0$. Nevertheless we expect to have $\sigma_x \approx 0$, $\sigma_y \approx 0$, $\sigma_z \approx 0$, for small times T_{F_1}, and this will imply to obtain

$$\tilde{e}_{x_{2r}} = -\tilde{c}\,\tilde{e}_{x_{1r}}, \quad \tilde{e}_{y_{2r}} = -\tilde{b}\,\tilde{e}_{y_{1r}}, \quad \tilde{e}_{z_{2r}} = -\tilde{d}\,\tilde{e}_{z_{1r}}$$

whose solutions will be given as

$$\begin{aligned}\tilde{e}_{x_{1r}} &= \exp\left(-\tilde{c}\,(t - T_{F_1})\right)\tilde{e}_{x_{1r}}(T_{F_1}) \\ \tilde{e}_{y_{1r}} &= \exp\left(-\tilde{b}\,(t - T_{F_1})\right)\tilde{e}_{y_{1r}}(T_{F_1}) \\ \tilde{e}_{z_{1r}} &= \exp\left(-\tilde{d}\,(t - T_{F_1})\right)\tilde{e}_{z_{1r}}(T_{F_1})\end{aligned}$$

Consequently this implies that $x_{1r} \to x_{1r}(0)$, $y_{1r} \to y_{1r}(0)$, $z_{1r} \to z_{1r}(0)$ and $x_{2r} \to 0$, $y_{2r} \to 0$, $z_{2r} \to 0$.

Note that (17) can be also written as

$$\begin{aligned}\dot{x}_{1r} &= x_{2r} \quad \dot{x}_{2r} = \tilde{u}_x \\ \dot{y}_{1r} &= y_{2r} \quad \dot{y}_{2r} = \tilde{u}_y \\ \dot{z}_{1r} &= z_{2r} \quad \dot{z}_{2r} = \tilde{u}_z\end{aligned} \tag{20}$$

$\forall\ T_{F_1} \leq t \leq T_F$.

Coupling the trajectories

The idea is to design only one trajectory to perform the mission. Switching between two trajectories programmed separately could be a problem when the vehicle is moving fast enough. Therefore, we can propose the following general trajectory

$$\begin{aligned}\dot{x}_{1r} &= x_{2r} \quad \dot{x}_{2r} = g_1(t)u_x + f_1(t)\tilde{u}_x \\ \dot{y}_{1r} &= y_{2r} \quad \dot{y}_{2r} = g_1(t)\,u_y + f_1(t)\tilde{u}_y \\ \dot{z}_{1r} &= z_{2r} \quad \dot{z}_{2r} = g_1(t)\,u_z + f_1(t)\tilde{u}_z\end{aligned} \tag{21}$$

where $g_1(t)$ and $f_1(t)$ are given by

$$f_1(t) = \begin{cases} e^{(n(t-T_{F_1}))} & 0 \leq t < T_{F_1} \\ 1 & T_{F_1} \leq t \leq T_F \end{cases} \tag{22}$$

$$g_1(t) = \begin{cases} 1 - f_1(t) & 0 \leq t < T_{F_1} \\ 0 & T_{F_1} \leq t \leq T_F \end{cases} \tag{23}$$

with $n > 0$.

From Figure 6 observe that when n increases its value, during almost all the entire interval time $0 \leq t < T_{F_1}$, $f_1(t)$ remains small and almost zero, even when t takes values close to T_{F1}. Therefore, it is possible to consider that for all $0 \leq t < T_{F_1}$, $f_1(t)$ and $g_1(t)$ could be given by

$$f_1(t) \approx 0; \quad g_1(t) = 1 - \underbrace{f_1(t)}_{\approx 0} \approx 1$$

assuring that for $0 \leq t < T_{F_1}$ and with high values of $n > 0$, the system (21) has similar dynamics that (16).

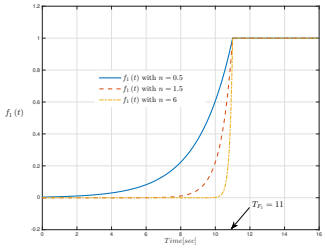

Fig. 6. $f_1(t)$ for different values of $n > 0$

Finally for the interval time $T_{F_1} \leq t \leq T_F$ and from (22) and (23), it yields

$$f_1(t) = 1; \quad g_1(t) = 0$$

Implying that system (21) is the same that (20), this signifies that (21) takes the same dynamics for returning at the base station with coordinates $(x_{1r}(0), y_{1r}(0), z_{1r}(0))$.

Hence it was proved that the system (21) takes two different dynamics for all the interval time $0 \leq t \leq T_F$.

Numerical validation:

Consider the mission given in section III with same characteristics. The objective is to include the trajectory to return to the base station $(x_{1r}(0), y_{1r}(0), z_{1r}(0)) = (-3, 5, 0)$ at time $T_{F_1} = 11$. The gains for the final phase are $\tilde{c} = 2$, $\tilde{b} = 3$, $\tilde{d} = 4$, $\tilde{k}_x = 2$, $\tilde{k}_y = 4$, $\tilde{k}_z = 4$ for satisfying (20).

In Figure 7 the two different dynamics can be analyzed, notice that both are executed at the interval time $0 \leq t < T_{F_1}$ and $T_{F_1} \leq t \leq T_F$.

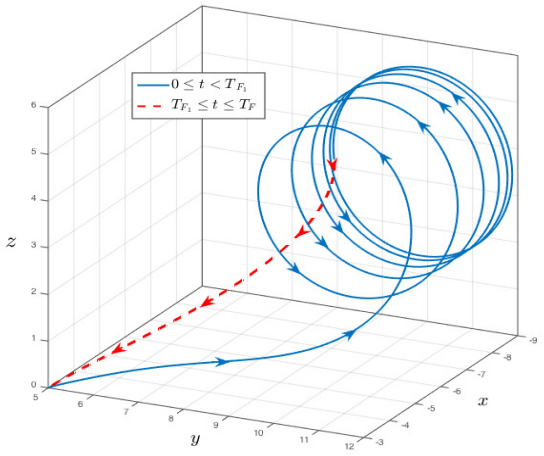

Fig. 7. Dynamics (x_{1r}, y_{1r}, z_{1r}) with acrobatic motion around (x_{eq}, y_{eq}, z_{eq}) and return to $(x_{1r}(0), y_{1r}(0), z_{1r}(0))$.

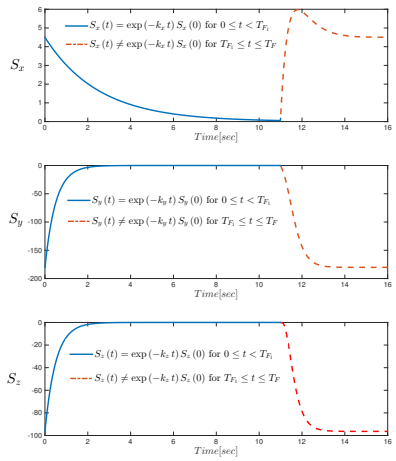

Fig. 8. S_x, S_y and S_z performance at the interval time $0 \leq t \leq T_F$.

In Figure 8 the asymptotic convergence of S_i can be appreciated, this convergence occurs only at the interval time $0 \leq t < T_{F_1}$, where this guarantees that (x_{1r}, y_{1r}, z_{1r}) will do the acrobatic maneuver around (x_{eq}, y_{eq}, z_{eq}). For $T_{F_1} \leq t \leq T_F$, we can notice that the asymptotic convergence around zero is lost for S_i, meaning that the first dynamic has been switched to the return dynamic. Similarly in Figure 9 the σ_i convergence to zero is presented for all $T_{F_1} \leq t \leq T_F$.

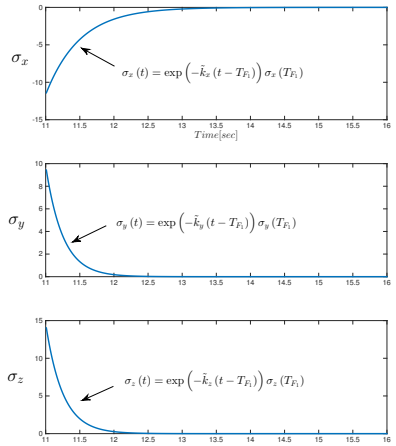

Fig. 9. Asymptotic convergence of σ_x, σ_y and σ_z $\forall$ $T_{F_1} \leq t \leq T_F$.

IV. Trajectory Tracking Control

The control challenge will be to track the proposed trajectory (x_{1r}, y_{1r}, z_{1r}) using the dynamics of a quadrotor vehicle. Remember that the vehicle evolutes in 3D with coordinates x, y, z and angles ψ, θ, ϕ for yaw, pitch and roll respectively.

Then, define $e_{x_1} = x_1 - x_{1r}$; $e_{y_1} = y_1 - y_{1r}$ and $e_{z_1} = z_1 - z_{1r}$ with $x_1 = x$, $y_1 = y$, $z_1 = z$, $\dot{x}_1 = x_2$, $\dot{y}_1 = y_2$ and $\dot{z}_1 = z_2$. Therefore from the quadrotor dynamics, see [22], it follows that

$$\begin{aligned}
\dot{e}_{x_1} &= e_{x_2}; & \dot{e}_{x_2} &= -\sin(\theta_1)\frac{1}{m}U_1 - \delta_x \\
\dot{e}_{y_1} &= e_{y_2}; & \dot{e}_{y_2} &= \cos(\theta_1)\sin(\phi_1)\frac{1}{m}U_1 - \delta_z \\
\dot{e}_{z_1} &= e_{z_2}; & \dot{z}_2 &= \cos(\theta_1)\cos(\phi_1)\frac{1}{m}U_1 - \delta_z
\end{aligned}$$

with $\delta_x = g_1(t)\,u_x + f_1(t)\,\tilde{u}_x$, $\delta_y = g_1(t)\,u_y + f_1(t)\,\tilde{u}_y$ and $\delta_z = g + g_1(t)\,u_z + f_1(t)\,\tilde{u}_z$. m is the mass of the aerial vehicle and U_1 defines the control input.

Propose U_1 as

$$U_1 = \frac{m\, r_z}{\cos(\theta_{1r})\cos(\phi_{1r})} \tag{24}$$

then for assuring convergence of the translation errors to zero, the following relations are obtained

$$\phi_{1r} = \tan^{-1}\left(\frac{r_y}{r_z}\right) \tag{25}$$

$$\theta_{1r} = \tan^{-1}\left\{(-1)\cos(\phi_{1r})\left(\frac{r_x}{r_z}\right)\right\} \tag{26}$$

and

$$\phi_{2r} = \frac{\cos^2(\phi_{1r})}{r_z}\left[\dot{r}_y - \dot{r}_z\tan(\phi_{1r})\right] \tag{27}$$

$$\theta_{2r} = \frac{\cos^2(\theta_{1r})}{r_z}\left[r_x\sin(\phi_{1r})\,\phi_{2r} - \dot{r}_z\tan(\theta_{1r}) - \dot{r}_x\cos(\phi_{1r})\right] \tag{28}$$

with $r_x = \delta_x + V_x$; $r_y = \delta_y + V_y$; $r_z = \delta_z + V_z$; and $V_x = k_{p_x}e_{x_1} + k_{d_x}e_{x_2}$; $V_y = k_{p_y}e_{y_1} + k_{d_y}e_{y_2}$; and $V_z = k_{p_z}e_{z_1} + k_{d_z}e_{z_2}$.

If $\phi_1 \to \phi_{1r}$, $\theta_1 \to \theta_{1r}$ and $\psi_1 \to \psi_{1r}$ then this will imply that $e_{x_i}, e_{y_i}, e_{z_i} \to 0$. Therefore, the following objective is to define a robust controller to assure the convergence of the orientation to the desired values.

The attitude dynamics of the quadrotor, see [22], can be written in the errors terms as

$$\begin{aligned}
\dot{e}_{\phi_1} &= e_{\phi_2}; \quad \dot{e}_{\phi_2} = \bar{f}_1 + b_1U_\phi + \xi_1 \\
\dot{e}_{\theta_1} &= e_{\theta_2}; \quad \dot{e}_{\theta_2} = \bar{f}_2 + b_2U_\theta + \xi_2 \\
\dot{e}_{\psi_1} &= e_{\psi_2}; \quad \dot{e}_{\psi_2} = \bar{f}_3 + b_3U_\psi + \xi_3
\end{aligned}$$

with $e_{\phi_1} = \phi_1 - \phi_{1r}$, $e_{\theta_1} = \theta_1 - \theta_{1r}$, $e_{\psi_1} = \psi_1 - \psi_{1r}$, $\dot{e}_{\phi_1} = e_{\phi_2} = \phi_2 - \dot{\phi}_{1r}$, $\dot{e}_{\theta_1} = e_{\theta_2} = \theta_2 - \dot{\theta}_{1r}$, $\dot{e}_{\psi_1} = e_{\psi_2} - \dot{\psi}_{1r}$ where $\phi_1 = \phi$, $\theta_1 = \theta$, $\psi_1 = \psi$, $\dot{\phi}_1 = \phi_2$, $\dot{\theta}_1 = \theta_2$, $\dot{\psi}_1 = \psi_2$. U_j, $j : \phi, \theta, \psi$ represents the attitude control input and ξ_i, $i : 1, 2, 3$ means an external and unknown perturbation.

In addition,

$$\bar{f}_1 = \left(e_{\theta_2} + \dot{\theta}_{1r}\right)\left(e_{\psi_2}\gamma_1 - \beta_1\right) - \ddot{\phi}_{1r}$$

$$\bar{f}_2 = \left(e_{\phi_2} + \dot{\phi}_{1r}\right)\left(e_{\psi_2}\gamma_2 - \beta_2\right) - \ddot{\theta}_{1r}$$

$$\bar{f}_3 = \left(e_{\theta_2} + \dot{\theta}_{1r}\right)\left(e_{\phi_2} + \dot{\phi}_{1r}\right)\gamma_3 - \ddot{\psi}_{1r}$$

where $\gamma_1 = \left(\frac{I_y - I_x}{I_x}\right)$, $\gamma_2 = \left(\frac{I_z - I_x}{I_y}\right)$, $\gamma_3 = \left(\frac{I_x - I_y}{I_z}\right)$, $\beta_1 = \frac{I_r}{I_x}\Omega$, $\beta_2 = \frac{I_r}{I_y}\Omega$, $b_1 = \frac{l}{I_x}$, $b_2 = \frac{l}{I_y}$, $b_3 = \frac{l}{I_z}$.

The distance between each motor to the gravity center of the vehicle is denoted by l. The inertia of the vehicle in each axis is defined by I_x, I_y and I_z while the inertia of the motor is represented by I_r, the speed of the rotor is defined by Ω. For our mission the vehicle is not changing in heading then the desired yaw angle is considered constant $\dot{\psi}_{1r} = \ddot{\psi}_{1r} = 0$.

Defining the next sliding functions S_i as $S_1 = e_{\phi_2} + M_{11}e_{\phi_1}$, $S_2 = e_{\theta_2} + M_{22}e_{\theta_1}$ and $S_3 = e_{\psi_2} + M_{33}e_{\psi_1}$. Then, $\dot{S}_1 = \bar{f}_1 + b_1U_\phi + \xi_1 + M_{11}e_{\phi_2}$, $\dot{S}_2 = \bar{f}_2 + b_2U_\theta + \xi_2 + M_{22}e_{\theta_2}$ and $\dot{S}_3 = \bar{f}_3 + b_3U_\psi + \xi_3 + M_{33}e_{\psi_2}$. For eliminating the linear part in $\dot{S}_i$ and achieving asymptotic convergence, propose

$$U_\phi = b_1^{-1}\left(\bar{u}_1 - M_{11}e_{\phi_2}\right), U_\theta = b_2^{-1}\left(\bar{u}_2 - M_{22}e_{\theta_2}\right),$$
$$U_\psi = b_3^{-1}\left(\bar{u}_3 - M_{33}e_{\psi_2}\right)$$

with positive gains M_{11}, M_{22} and M_{33}. For assuring that $e_{\phi_1} \to 0$, $e_{\theta_1} \to 0$, $e_{\psi_1} \to 0$ asymptotically in presence of unknown and bounded disturbances ξ_i, i.e., $|\xi_i| \leq L_i$, we propose the following integral sliding mode controls

$$\bar{u}_1 = -\rho_1 \text{Sign}\left(S_1 - Z_1\right) - k_1 S_1 \quad (29)$$
$$Z_1 = -k_1 \int S_1 dt \quad (30)$$

with $Z_1(0) = S_1(0)$ and $\rho_1 = \alpha_1 + \left|\bar{f}_1\right| + L_1$.

$$\bar{u}_2 = -\rho_2 \text{Sign}(S_2 - Z_2) - k_2 S_2 \quad (31)$$
$$Z_2 = -k_2 \int S_2 dt \quad (32)$$

with $Z_2(0) = S_2(0)$ and $\rho_2 = \alpha_2 + \left|\bar{f}_2\right| + L_2$.

$$\bar{u}_3 = -\rho_3 \text{Sign}\left(S_3 - Z_3\right) - k_3 S_3 \quad (33)$$
$$Z_3 = -k_3 \int S_3 dt \quad (34)$$

with $Z_3(0) = S_3(0)$ and $\rho_3 = \alpha_3 + \left|\bar{f}_3\right| + L_3$.

Observe that $-\rho_i \,\text{Sign}(S_i - Z_i)$ compensates $\bar{f}_i + \xi_i$ for all $t \geq 0$ if and only if $Z_i(0) = S_i(0)$. Notice also that each term $-k_i S_i$ achieves to do $S_i \to 0$ asymptotically for all $t \geq 0$.

Trajectory-control scheme validation

The pillar is placed at $(x_{eq}, y_{eq}, z_{eq}) = (4, 0, 4)$m and the quadrotor initial position is $(x_{1_0}, y_{1_0}, z_{1_0}) = (0, 0, 0)$m with the initial condition for velocity as $(x_{2_0}, y_{2_0}, z_{2_0}) = (0, 0, 0)$m/sec. The aerial vehicle must to return at the base station at time $T_{F_1} = 11$sec. The gains used for coupling the two trajectories (acrobatic trajectory and return to the base station) are the same that considered previously. For validating the control scheme, the gains are $\alpha_1 = \alpha_2 = \alpha_3 = 0.1$, $k_1 = 5$, $k_2 = 3$ and $k_3 = 5$.

In Figure 10 we can observe the well performance of the quadrotor when tracking the desired trajectory (x_{1r}, y_{1r}, z_{1r}). In Figure 11, the ϕ_1 performance is illustrated, note here that $\phi_1 \to \phi_{1r}$ since the beginning. This signifies that the dynamics represented into the interval time $0 \leq t < (T_{F_1} = 11sec)$ give a spiral trajectory, with center at $(x_{eq}, y_{eq}, z_{eq}) = (4, 0, 4)m$, that is followed by the quadrotor. Note that in the transition time $T_{F_1} = 11$sec,

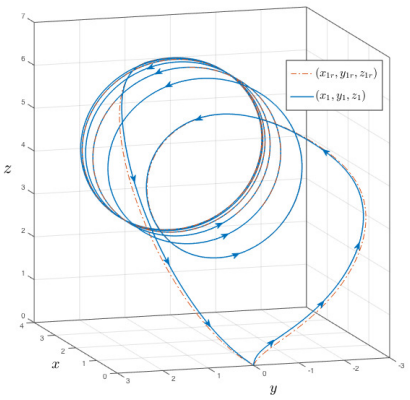

Fig. 10. Vehicle response when tracking the desired trajectory (x_{1r}, y_{1r}, z_{1r}).

the roll dynamics ϕ_1 is modified, this means that the aerial vehicle returns at the base station. In this figure it is possible to appreciate the agressive maneuvers that the quadrotor does for tracking the desired trajectory. The pitch behavior is presented in Figure 12, notice that this performance is close to zero. It is cause the maneuver is only done in the roll angle. The performance on these angles at time $T_{F_1} = 11$sec is given when the vehicle returns to the base station.

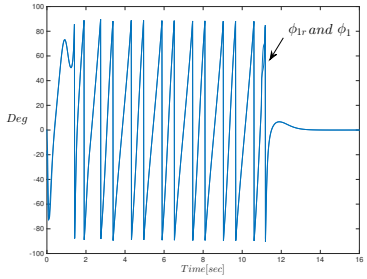

Fig. 11. ϕ_1 and ϕ_{ir} performance. Observe the agressives angles reached by the quadrotor.

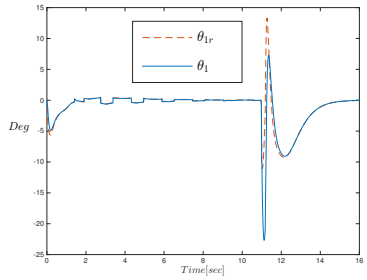

Fig. 12. θ_1 and θ_{1r} convergence. As expected this angle is close to zero because in the trajectory only the roll angle is used.

In Figure 13 the position control input response U_1 is represented and in Figure 14 the behavior controllers U_ϕ, U_θ & U_ψ are depicted. These controllers are responsible to do that the quadrotor tracks the desired dynamics (x_{1r}, y_{1r}, z_{1r}).

V. Conclusion

A special trajectory for aerial acrobatics maneuvers were developed in this paper. The trajectory was conceived using

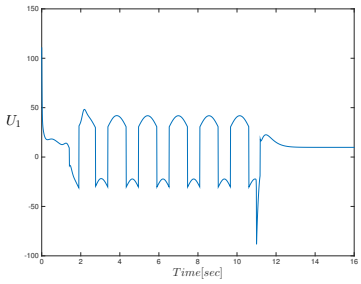

Fig. 13. U_1 control input response.

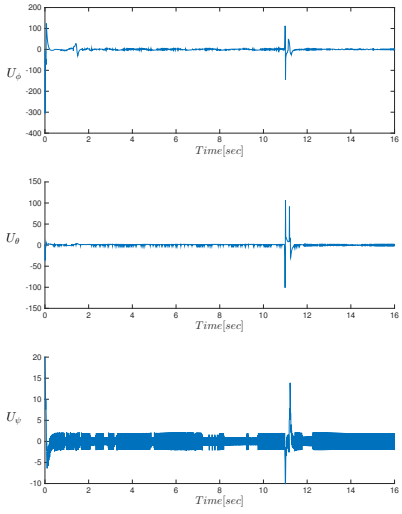

Fig. 14. U_ϕ, U_θ and U_ψ performance

the bifurcation theory and the sliding mode approach. The goal of this trajectory is to do spiral loops around a point in the 3D space and return to the base station. For achieving a desired angular velocity around the stable limit cycle solution, the parameter gamma was introduced in the trajectory. An integral sliding mode control was introduced for tracking the proposed trajectory. Numerical results have shown the well performance of the proposed trajectory-control scheme.

Future work includes the real-time validation in our platforms.

REFERENCES

[1] Martin, P., Devasia, S., Paden B., A different look at output tracking: control of a VTOL aircraft, Automatica, 1(32), 101–107,1996.

[2] Sujit, P.B. and Saripalli, S. and Borgues-Sousa, J., Unmanned Aerial Vehicle Path Following, IEEE Control Systems Magazine, 1(34), pp. 42 – 59, 2014.

[3] Zuo, Z., Trajectory tracking control design with command-filtered compensation for a quadrotor, IET Control Theory and Application, 4(11), pp. 2343 – 23559, 2010.

[4] Raffo, G. and Ortega, M. G. and Rubio, F. R., Backstepping/Nonlinear H_∞ Control for Path Tracking of a QuadRotor Unmanned Aerial Vehicle ,Proceedings of the American Control Conference, pp. 3356-3361, Seattle, Washington, USA, June 11-13, 2008

[5] Aguilar, A.P. and Hespanha, J.P., Trajectory-Tracking and Path-Following of Underactuated Autonomous Vehicles With Parametric Modeling Uncertainty, IEEE Transactions on Automatic Control, 8(52), pp. 1362 – 1379, 2007.

[6] Nelson, D.R. and Blake Barber, D. and McLain, T. and Beard, R.W., Vector Field Path Following for Miniature Air Vehicles, IEEE Transactions on Robotics, 3(23), pp. 519–529, 2007.

[7] Hamel, T. and Mahony, R. and Chriette, A, Visual servo trajectory tracking for a four rotor VTOL aerial vehicle, Proceedings of the 2002 International Conference on Robotics & Automation, pp. 2781–2786, Washington, DC, USA, 2002

[8] Jin Kim, H. and Shim, D.H. and Sastry, S., Nonlinear Model Predictive Tracking Control for Rotorcraft-based Unmanned Aerial Vehicles, Proceedings of the American Control Conference, pp. 3576-3581, Anchorage, AK May 8-10, 2002.

[9] Ren, W. and Beard, R.W., Trajectory Tracking for Unmanned Air Vehicles With Velocity and Heading Rate Constraints, IEEE Transactions on Control System and Technology, 12(5), pp. 706-716, 2004.

[10] Hehn, M. and D'Andrea, R., Quadrocopter Trajectory Generation and Control, 8th World Congress the International Federation of Automatic Control, pp. 1485–1491, Milano, Italy, 2011.

[11] Prodan, I. and Olaru, S., and Bencatel, R. and Borges de Sousa, J., and Stoica, C. and Niculescu, S-I, Receding horizon flight control for trajectory tracking of autonomous aerial vehicles, Control EngineeringPractice, 21, pp. 1334–1349, 2013.

[12] Kamel M., Burri M. and Siegwart R., Linear vs Nonlinear MPC for Trajectory Tracking Applied to Rotary Wing Micro Aerial Vehicles, 20th IFAC World Congress, 50(1), pp. 3463-3469, 2017.

[13] Eltayeb, A., Rahmat, M.F., and Basri, M.A., Eltoum, M. A M. and El-Ferik, S., An Improved Design of an Adaptive Sliding Mode Controller for Chattering Attenuation and Trajectory Tracking of the Quadcopter UAV, IEEE Access, (8), pp. 205968-205979, 2020.

[14] Wang, N. and Choon Ki A., Coordinated Trajectory-Tracking Control of a Marine Aerial-Surface Heterogeneous System, IEEE/ASME Transactions on Mechatronics, 26(6), pp. 3198-3210, 2021.

[15] Baca, T., Hert, D., Loianno, G., Saska, M., and Kumar, V., Model Predictive Trajectory Tracking and Collision Avoidance for Reliable Outdoor Deployment of Unmanned Aerial Vehicles, 2018 IEEE/RSJ International Conference on Intelligent Robots and Systems (IROS), pp. 6753-6760, 2018.

[16] Marsden, J.E., and McCracken, M., The Hopf bifurcation and its applications, Springer Science & Business Media, 2012. ISBN: 1461263743.

[17] Hubbard, JH and West, BH, Differential Equations: A Dynamical Systems Approach-Higher-Dimensional Systems, Springer, 1995.

[18] Jordan, D.W., and Smith, P., Nonlinear ordinary differential equations: an introduction to dynamical systems, Oxford University Press, USA, 1999. ISBN: 0198565623.

[19] Drakunov, S.V. and Utkin, V.I., Sliding mode control in dynamic systems, International Journal of Control, 55(4), pp. 1029–1037, 1992.

[20] Edwards, C.r and Spurgeon, S., Sliding mode control: theory and applications, Crc Press, 1998. ISBN: 0748406018.

[21] Shtessel, Y and Edwards, C and Fridman, L and Levant, A., Sliding Mode Control and Observation, Birkhäuser, 2014.

[22] Castillo, P. and Munoz, L-E. and Garcia, P, Indoor Navigation Strategies for Aerial Autonomous Systems, Elsevier, 2017. ISBN: 9780128051894.